Saturation mechanism in clarinet-like instruments, the effect of the localised non-linear losses

Merouane Atig, Jean-Pierre Dalmont, Joël Gilbert

Saturation mechanism in clarinet-like instruments, the effect of the localised non-linear losses.

Mérouane Atig*, Jean-Pierre Dalmont, Joël Gilbert

Laboratoire d'Acoustique de l'Université du Maine (LAUM – UMR CNRS 6613)

Av. O. Messiaen, 72085 Le Mans cedex 9, France

Abstract

The question of what limits the amplitude of the oscillations of clarinet-like instruments is investigated. The study is based on numerical simulations in which two kind of losses are taken into account: linear losses and non-linear losses localised at the open end of the tube. The influence of the amount of losses on the saturation process and on the playing range of clarinet-like instruments is shown. Results are confirmed by experiments using an artificial mouth in which the non-linear losses are varied using several terminations with different geometries.

1 Introduction

Many papers have been devoted to single-reed instruments (for a first overview, see for example Nederveen [1], Fletcher and Rossing [2], Hirschberg [3], Kergomard [4]). These papers can be classified in two groups. In the first group, papers are dedicated to the study and modelling of a specific part of the instrument (acoustical resonator part, mechanical behaviour of the reed, hydrodynamic behaviour of the air entering into the mouthpiece). In the second group, papers are dedicated to the oscillation behaviour of the instrument under playing conditions. The first attempt to derive theoretically periodic oscillation regimes defined by their fundamental frequency and their spectrum is due to Worman [5]. His results are at the origin of many works, such as the one by Benade and Kouzoupis [6] who derived semi-empirical formulae fitted with experimental results. Mc Intyre et al [7] have shown how musical instruments like bowed string and wind instruments can be modelled as a non-linear closed feedback loop operating in free oscillations. More recently Grand et al [8] have extended Worman's work in order to find both the nature of the bifurcation of the trivial solution depending

*Corresponding author. Tel: +33-2-4383-3681; fax: +33-2-4383-3520. *E-mail adress:* merouane.atig@univ-lemans.fr

on the excitator and the resonator characteristics, and the spectrum of the small periodic oscillations in the direct bifurcation case. On the other hand, great attention has been paid to lossless models, the solutions of which are squared signals, analogue to the Helmholtz motion in string instruments. These two approaches have been linked in [9]. In all these works attention is focused on the permanent regime and its stability and especially on the threshold of oscillation, that is the minimum mouth pressure for which oscillations occur.

The question of what limits the amplitude of the oscillations, although essential for the musician, has been somewhat neglected. The importance of reduced nonlinear losses to extending the playing range of a clarinet by rounding its corners has been reported in [10] referring to the study of Benade and Cuddeback [11]. By playing experiments before and after rounding the corners of clarinet tone holes and joint edges, the dynamic range is extended. More recently this point has been discussed in [12]. In this paper it is shown that, due to losses the pressure in the mouthpiece becomes too low to ensure the reopening of the reed or at least to ensure a sufficient reed opening to provide the flow needed to sustain the oscillation. In this paper it is also suggested that linear losses (viscothermal losses in the tube) are not sufficient to explain the low value of the maximum mouth pressure for which there is extinction of periodic oscillations.

As pointed out by Hirschberg in [3], non-linear behaviour due to flow separation and vortex shedding should certainly be expected in the open holes and terminations of woodwinds under realistic playing conditions. Although systematic studies of extra losses at open-ended tubes have been carried out in the past (see for example Ingard [13], Disselhorst [14], Peters [15]), it is not a priori obvious what the impact of these phenomena is on the sound production produced by wind instruments. Notice that Bouasse [16] said that the horn of brass instruments might reduce vortex shedding at the pipe end. More recently Coltman [17] measured that non linear turbulent losses are substantial, and said that in any quantitative treatment of the flute as an oscillation system, these non linear losses must be taken into account. One of the aims of the present paper is to investigate how non-linear losses at the open end of a pipe influence the playing range of the instrument.

The role of non-linear losses in the operation of a wind instrument has been mentioned in some papers [1, 3, 18]. It is now clear that the bad operation of the puzzling "silent clarinet" described in Benade and Keefe [19] (a clarinet with small and short holes which has the same input impedance as a standard clarinet) is due to non-linear effects in side holes [19, 20]. Non-linear losses may also be a main cause of the sound level difference between a baroque flute and a modern flute [21, 22] and more generally between wind instruments with small holes (baroque instruments) and wind instruments with large holes (Boehm instruments). It is not the subject of the present paper to investigate the question of the side holes but only to show that non linear losses may have an influence on the playing range of a wind instrument.

In a wind instrument, non-linear losses are proportional to the hole cross-section, and also depend on the

hole geometry [20]. In particular the radius of curvature of the edges have a great influence on the losses: the more rounded the edges, the smaller the losses [23]. In the present study, the first open hole is the open end of a straight tube, and the effects of variation of the diameter of a side hole are not studied. In order to vary the influence of non-linear losses, only the radius of curvature of the pipe end is varied. The study of the non-linear losses induced by the different terminations has been the object of a specific study [23] of which the main results are summarised in section 2.

To investigate this, two tools are used. The first tool is an experimental setup including an artificial blowing machine. This blowing machine has been used in previous studies [9, 24, 25, 26]. The clarinet is replaced here with a straight cylinder, the termination of which can be modified in order to vary the non-linear loss parameters. The following experiments are done for different pipe terminations. Starting from zero, the pressure is increased until oscillations starts and then stops. Then the pressure is decreased until oscillations starts and then stops again. During these experiments both the mouthpressure and the pressure in the mouthpiece are measured.

The second tool is a numerical simulation. This simulation is based on the "simplest" model of a clarinet mouthpiece. Despite its simplicity this model has been validated with experiments. The values of the parameters used in the simulation are deduced from experiments [25]. The clarinet is modelled as a an open cylinder with frequency-independent losses (the model is called "Raman's" model in [27]).The sample frequency is the lowest possible: the time step used for the simulation is half of the period of the oscillation. Finally this simulation is modified in order to include non-linear losses at the end of the pipe. The value of the parameter on which the non-linear losses depend is also deduced from experiments [23]. Results are analysed and compared with experiments.

The present paper is divided into five sections. After this brief introduction, the theoretical background is presented in section 2. A simplified physical model of the clarinet-like instrument and the simulation method for calculating the acoustical oscillations are summarized in section 2.1 and 2.2. A first attempt to take into account localised non-linear losses in the model and the modified simulation method are presented in section 2.3 and 2.4. The experimental device and procedure are described in section 3. The experiments are performed using a clarinet-like instrument coupled to an artificial mouth, the clarinet-like instrument being a clarinet mouthpiece fitted to a cylindrical tube with different terminations described in section 3.1, then the estimation from the experiments of the parameters for the simulations is given in section 3.2. The results of the measurements are compared with the theoretical results obtained with the simulations in section 3.3. Finally the perspectives of this work are discussed in the conclusion, section 4.

2 Theory

2.1 Elementary model

The "simplest" model of a clarinet is made up with only two equations: one for the non-linear excitation mechanism (reed-mouthpiece system) and one for the resonator, usually regarded as a linear system. The two equations make the coupling between the two following variables: $u(t)$, the volume flow entering into the instrument, and $p(t)$, the acoustical pressure in the mouthpiece (Fig. 1).

[Figure 1 about here.]

The first equation gives the volume flow at the input of the instrument:

$$u = S_j \sqrt{\frac{2\Delta p}{\rho}}, \tag{1}$$

where S_j is the cross section of the jet created at the end of the reed channel and ρ the density of the air. Δp is the pressure difference between the mouth and the mouthpiece. It is derived from the Bernoulli equation assuming a turbulent dissipation of the energy in the jet without recovery of pressure (in a quasi-stationary approximation) [3]. Δp is related to the acoustic pressure $p(t)$ by:

$$\Delta p = P_m - p(t) \tag{2}$$

where P_m is the mouth pressure which is assumed to be constant. The jet cross section is assumed to be proportional to the reed opening H:

$$S_j = wH \tag{3}$$

where w is the effective width of the reed channel (for experimental evidences see Dalmont et al [25]). Ignoring the dynamics of the reed, the reed opening variation is assumed to be proportional to the pressure difference Δp which leads to

$$u = w(H_0 - \frac{\Delta p}{k})\sqrt{\frac{2\Delta p}{\rho}} \tag{4}$$

where H_0 is the reed opening at rest ($P_m = 0$) and k the reed stiffness. Moreover, if the pressure difference is larger than a limit value P_M, the reed is supposed to close the opening ($H = 0$) and the flow entering into the mouthpiece is equal to zero. The limit value P_M for which the reed closes the opening is given by $P_M = kH_0$. It is the minimum value of the mouth pressure for which the static solution corresponding to the reed blocked against the lay is stable. Finally the volume flow u can be written as a non-linear function of the acoustic

pressure p:

$$u = \begin{cases} wH_0(1 - \frac{P_m - p}{P_M})\sqrt{\frac{2(P_m - p)}{\rho}} & \text{if} \quad P_m - p \leq P_M, \\ 0 & \text{if} \quad P_m - p \geq P_M. \end{cases} \tag{5}$$

In Dalmont et al [25] it is shown that the model corresponds reasonably to reality except that in practice the reed channel seems to be never completely closed.

The resonator is classically described in the frequency domain (ω being the angular frequency) by its input impedance $Z(\omega) = P(\omega)/U(\omega)$, where $P(\omega)$ and $U(\omega)$ are the Fourier transform of the pressure $p(t)$ and the volume velocity $u(t)$, respectively. Yet, in this paper, the input impedance of the resonator is defined as $Z(\omega) = P(\omega)/V(\omega)$, where $V(\omega)$ is the Fourier transform of the acoustic velocity averaged over the cross sectional area of the tube $v(t) = u(t)/S$. However, the resonator can be described in the time domain too, using its impulse response $h(t)$, where $h(t)$ is the inverse Fourier transform of the impedance:

$$p(t) = h(t) * v(t) = \int_{-\infty}^{\infty} h(t - s)v(s)ds. \tag{6}$$

2.2 Simulation method

In order to calculate the oscillations, a discrete-time simulation technique in is adapted from Schumacher [28]. Direct numerical integration of the convolution equation, Eq. (6), would be time-consuming; using the reflection function $r(t)$ is more efficient than using the impulse response. The reflection function is the inverse Fourier transform of the reflection coefficient $R(\omega)$ defined from the impedance as follows:

$$R(\omega) = \frac{Z(\omega) - \rho c}{Z(\omega) + \rho c} \tag{7}$$

where ρc is the characteristic impedance of the cylindrical tube. After some algebra, the convolution equation, Eq. (6), is rewritten as follows:

$$p(t) = \rho c\, v(t) + r(t) * (p(t) + \rho c\, v(t))\,. \tag{8}$$

To get further into simplification the clarinet is approximated with a pure cylinder open at the end. Ignoring losses, the reflection function is a delayed Dirac function:

$$r(t) = -\delta(t - 2\tau) \tag{9}$$

where $\tau = L/c$, L being the length of the tube and c the speed of sound in free space. In that case, Eq. (8) can simply be replaced by:

$$p(t) = \rho c\, v(t) + p_{inc}, \tag{10}$$

with $p_{inc} = -p(t-2\tau) - \rho c\, v(t-2\tau)$. Eq. (10) says that $p(t)$ is proportional to the volume current at the instant, plus the "incident" pressure wave p_{inc} from the open end, which represents the increasingly dim memory the system has of its past [28]. The two Eqs. (5–10) yield a non linear equation with only one unknown at the present time t, the acoustical pressure $p(t)$:

$$p(t) - \rho c\, F_{NL}\{p(t)\} - p_{inc} = 0 \tag{11}$$

where F_{NL} is the non linear relationship defining $v(t)$ as a function of $p(t)$, Eq. (5), with $v(t) = u(t)/S$). In the case of the lossless cylindrical tube, assuming that the sampling frequency $F_s = 1/\Delta t$ is given by $F_s = 1/2\tau$ (i.e. $\Delta t = 2\tau$), Eq. (11) yields:

$$p[n] - \rho c\, F_{NL}\{p[n]\} + p[n-1] + \rho c\, F_{NL}\{p[n-1]\} = 0 \tag{12}$$

where $p[n]$ and $p[n-1]$ are the acoustical pressure at $t = n\Delta t = 2n\tau$ and $t = (n-1)\Delta t = 2(n-1)\tau$ respectively. Then, given as initial condition the acoustical pressure at $t = 0$, the acoustical pressure can be calculated step by step in time. This yields the periodic oscillations corresponding to the fundamental regime of the clarinet-like instrument using the lowest possible sample frequency (2 points per period of oscillations). As remarked by Mc Intyre et al [7], these simulations have been found capable of mimicking basic aspects of the strongly non-linear behaviour of the clarinet. Following them, Maganza et al [29] have exhibited sequences of period doubling; Kergomard in [4] carried out an extensive study of transient and periodic regimes of the clarinet-like instrument.

[Figure 2 about here.]

Until now the cylindrical tube has been considered lossless. Two kind of linear losses can be considered when studying the wind instruments: the viscothermal losses in the pipe and the radiation losses in its open end. For the lowest register of reed instruments, the quality factor of the resonator is mainly determined by the viscothermal losses. These losses can be described by the amplitude transmission coefficient β which is positive and slightly less than one, assuming losses independant of frequency. The positive and negative going plane wave pressures (Fig. 2) in the input (p_e^+ and p_e^- respectively) and in the open end of the pipe (p_s^+ and p_s^- respectively) are linked as follows to take into account the wave propagation and the attenuation along the propagation:

$$\begin{cases} p_s^+(t) = \beta p_e^+(t-\tau), \\ p_e^-(t) = \beta p_s^-(t-\tau). \end{cases} \tag{13}$$

This is valid without dispersion and assuming a loss parameter independent of the frequency. Then the reflection function assuming a total reflection at the end of the tube becomes a delayed Dirac function times

the transmission coefficient β squared:

$$r(t) = -\beta^2 \delta(t - 2\tau). \tag{14}$$

In that case Eq. (12) can be simply rewritten:

$$p[n] - \rho c \, F_{NL}\{p[n]\} + \beta^2 \left\{ p[n-1] + \rho c \, F_{NL}\{p[n-1]\} \right\} = 0. \tag{15}$$

Knowing that $p_e(t) = p_e^+(t) + p_e^-(t)$ and $\rho c v_e(t) = p_e^+(t) - p_e^-(t)$, p_{inc} is two times the negative going pressure $p_e^-(t)$ in the input of the pipe. Furthermore the reflection function $r(t)$ is the response of the negative going pressure $p_e^-(t)$ to a positive going pressure $p_e^+(t)$ being a Dirac function. Then p_{inc} can be written as follows:

$$p_{inc} = 2p_e^-(t) = r(t) * 2p_e^+(t). \tag{16}$$

In other words, p_{inc} can be obtained from $p_e^-(t)$ calculated as a function of $p_e^+(t)$.

Some typical simulated acoustical mouthpiece pressures are displayed in Fig. 3. The main parameter of the simulations is the mouth pressure P_m. If the simulation is run using a constant value of P_m, then a steady sound is obtained (Fig. 3(a)) after an initial transient due to the instantaneous variation from zero to P_m at the zero time. If P_m is slowly increasing, the simulation models a musical crescendo; and if P_m is slowly decreasing, the simulation models a musical decrescendo (Figs. 3(b), 3(c), 3(d)).

[Figure 3 about here.]

In order to compare the simulation results with the experimental ones, it is useful to display the envelope of the pressure fluctuations. The chosen sampling frequency F_s implies two samples per period of oscillation, and the fluctuating pressure is symmetrical, thus the envelope is easily obtained by displaying the absolute value of the simulated pressure. Fig. 4 shows the amplitude of the acoustical pressures displayed in Fig. 3 as a function of P_m (Figs. 4(a) and 4(b)). This display mode allows the comparison between the crescendo and decrescendo.

[Figure 4 about here.]

When a reed instrument is blown with an increasing mouth pressure (see Fig. 4(a)), the oscillation starts at a given pressure P_{thup} named "threshold of oscillation for increasing pressure". Then the amplitude increases with the mouth pressure, reaches a maximum, decreases, and stops suddenly at a pressure P_{extup} named "extinction threshold for increasing pressure". Above this pressure the reed is definitely closed. If now the pressure is decreased (Fig. 4(b)) the oscillation starts at a pressure P_{thdown} named "threshold of oscillation for decreasing pressure", and rises rapidly to a maximum amplitude. Then the amplitude decreases with

decreasing mouth pressure, and stops again at a pressure $P_{extdown}$ named "extinction threshold for decreasing pressure". P_{thup} is found from Fig. 4(a) to be close to 4400 Pa. It is significantly higher than P_{th} the threshold of instability of the reed equilibrium position ($P_{th} = 3350$ Pa). Obviously if the duration of the simulated crescendo is increased, then P_{thup} is decreasing toward the theoretical threshold P_{th}. P_{thdown} is found from Fig. 4(b) to be close to 8200 Pa. It is slightly lower than $P_M = 8500$ Pa. If the duration of the simulated decrescendo is increased, then P_{thdown} is increasing toward P_M.

The influence of the losses on the saturation mechanism is illustrated in Fig. 5. Simulations are done using different transmission coefficient β: the realistic value $\beta = 0.97$, and the other values $\beta = 0.96$ and $\beta = 0.94$. The simulations correspond to a tight embouchure ($P_M = 4000$ Pa). They are obtained for a mouth pressure P_m varying linearly from 150 Pa to 15000 Pa during 22.5 s (crescendo, Fig. 5(a)) and the other way round (decrescendo, Fig. 5(b)).

[Figure 5 about here.]

First, some conclusions can be drawn from the "crescendo" simulations (Fig. 5(a)). On the one hand it appears that the mouth pressure P_{extup} for which the oscillations stops is decreasing when the losses are increasing. It is infinite for $\beta = 1$ and decreases from 6800 Pa for $\beta = 0.97$, to 4600 Pa for $\beta = 0.94$, but remains higher than 4000 Pa, the value of P_M. It is clear that P_{extup} directly depends on the loss coefficient β. In contrast, the mouth pressure P_{thdown} for which the oscillations appear is not influenced by the losses (Fig. 5(b)). P_{thdown} remains always close to $P_M = 4000$ Pa when β is decreasing from 0.97 to 0.94. This hysteretic phenomenon shows that the clarinet-like system exhibits an inverse bifurcation — which is a typical scheme in non-linear dynamics [30, 31] — at the extinction. Analytical study is required for the derivation of the bifurcation diagram, and then to determine under which conditions this inverse bifurcation occurs.

2.3 Models for localised non-linear losses

In this subsection, a first attempt to take into account localised non-linear losses in the model is presented. Then the simulation technique in discrete time-domain presented in the previous subsection is adapted in the following section. When the acoustic displacement of the fluid particles becomes important, non-linear behaviour due to flow separation is expected, and extra non-linear losses have to be taken into account. Systematic studies of these extra losses in open-ended tubes have been carried out in the past: see for example pionnering works of Ingard [13, 32], and more elaborate theoretical and experimental work in Disselhorst [14] and Peters [15].

For low Strouhal numbers, i.e. high amplitudes of the acoustic velocity, Disselhorst [14] and Peters [15]

have developed a quasi-stationary model in order to describe the oscillating flow at the open pipe termination. During half a period, the acoustic velocity is oriented out of the tube and a jet-like outflow is assumed with a turbulent recovery region. During the second half-period, the acoustic velocity is oriented into the tube and there is a possible formation of a vena-contracta type of inflow with a turbulent recovery region. Acoustic energy is dissipated by the vortices in the turbulent mixing zones. The acoustic power P_{ac} dissipated in the vortices, averaged over a period of the acoustic oscillation, assuming a purely harmonic acoustic velocity, is found to be (Peters [15]):

$$P_{ac} = \frac{2c_d}{3\pi}\frac{1}{2}\rho v_{ac}^3 S \tag{17}$$

where S is the cross-sectional area of the tube and v_{ac} the amplitude of the acoustic velocity at the tube open end. The parameter c_d depends on the geometry of the pipe end, and is theoretically equal to 2 for a thin-walled unflanged pipe and to 13/9 for a flanged pipe with sharp edges. The acoustic power P_{ac} can also be expressed as a function of the termination impedance Z_{end}:

$$P_{ac} = \frac{1}{2}v_{ac}^2 S\,\mathrm{Re}(Z_{end}) \tag{18}$$

which leads, using Eq. (17), to:

$$\mathrm{Re}(\frac{Z_{end}}{\rho c}) = \frac{2c_d}{3\pi}\frac{v_{ac}}{c} \tag{19}$$

It should be noticed that the concept of impedance is theoretically valid only in the field of linear acoustics. It can be shown that the result given in Eq. (19) is strictly correct only in the case of a harmonic acoustic velocity.

2.4 Simulation method with non-linear losses

Now, non-linear losses have to be included in the simulation. The main simplification of our approach is the direct translation of the quasi stationary models to the unsteady case, by using the following boundary condition between the acoustic pressure p_s and the acoustic velocity averaged over the cross sectional area at the open end of the pipe v_s:

$$p_s(t) = \left(\frac{c_d}{2}\right)\frac{1}{2}\rho v_s^2(t)\,\mathrm{sgn}(v_s) \tag{20}$$

where $\mathrm{sgn}(v_s) = +1$ if the acoustic velocity v_s is oriented out of the pipe, and $\mathrm{sgn}(v_s) = -1$ if the acoustic velocity v_s is oriented into the pipe. From the boundary condition defined by Eq. (20), it is possible to check, in the case of a purely harmonic velocity, that the absorbed acoustic power P_{ac} averaged over a period of the acoustic oscillation is the same as the one expressed Eq. (17). Notice that when a clarinet is played, there is a mean flow which has not been taken into account in the discussion before. The clarinet being played at a

frequency close to a resonance frequency of the resonator, it is assumed that the mean flow is small compared with the amplitude of the acoustical velocity at the open end of the pipe. Then it is sensible to neglect the effect of the mean flow in our problem [33].

The simulation technique in discrete time-domain presented in the previous subsection has to be adapted to take into account the localised non-linear losses using Eq. (20). Because of the non-linear losses the pressure p_{inc} defined by Eq. (10) has to be calculated again. In other words following Eq. (16), the input negative going pressure p_e^- has to be calculated as a function of the input positive going pressure p_e^+. The boundary condition in the open end of the tube, Eq. (20), is written in terms of positive and negative going pressures:

$$p_s^- = -p_s^+ + \left(\frac{c_d}{2}\right)\frac{1}{2}\rho v_s^2\,\mathrm{sgn}(v_s). \tag{21}$$

If losses are small, the ideal open-end boundary condition is $p_s = 0$. Knowing that $p_s = p_s^+ + p_s^-$ and $\rho c v_s = p_s^+ - p_s^-$, v_s can be approximated by $v_s = 2p_s^+/\rho c$. As an example, considering $v_s = 30$ m/s and $c_d = 2$ leads to $(\frac{c_d}{2})\frac{1}{2}\rho v_s^2 \approx 540$ Pa which is small compared to p_s^+ in realistic situations ($p_s^+ \approx P_m > 5000$ Pa at high level). Using this approximation Eq. (21) can be replaced by

$$p_s^- = -p_s^+ + \left(\frac{c_d}{2}\right)\frac{1}{2}\rho\left(\frac{2p_s^+}{\rho c}\right)^2\mathrm{sgn}(p_s^+). \tag{22}$$

This equation combined with Eq. (13) leads to the relationship between the input negative going pressure p_e^- and the input positive going pressure p_e^+:

$$p_e^- = -\beta^2 p_e^+(t-2\tau)\left[1 - \beta c_d\frac{|p_e^+(t-2\tau)|}{\rho c^2}\right]. \tag{23}$$

Then the simulation method presented in section 2.1 remains effective by using the new definition of p_{inc} as a function of the delayed acoustical pressure $p(t-2\tau)$ and velocity $v(t-2\tau)$:

$$p_{inc} = -\beta^2[p(t-2\tau) + \rho c\, v(t-2\tau)]\left[1 - \beta c_d\frac{|p(t-2\tau) + \rho c\, v(t-2\tau)|}{\rho c^2}\right]. \tag{24}$$

In the discrete-time representation, the acoustical pressure is calculated step by step in time from solving the following Eq. (25) in place of Eq. (12):

$$p[n] - \rho c\, F_{NL}\{p[n]\} + \beta^2\{p[n-1] + \rho c\, F_{NL}\{p[n-1]\}\}\left[1 - \beta c_d\frac{|p[n-1] + \rho c\, F_{NL}\{p[n-1]\}|}{\rho c^2}\right] = 0. \tag{25}$$

Simulations are run in order to show the influence of the non linear losses on the saturation mechanism (see Fig. 6). The simulations are done with the same input parameters as above ($P_M = 4000$ Pa, P_m varying linearly from 150 Pa to 15000 Pa, crescendo, during 22.5 s). Comparing a simulation with linear losses only ($\beta = 0.97$) with a simulation where some non linear losses are added ($c_d = 1.7$), it appears that the extinction

mouth pressure P_{extup} is decreasing when the non linear losses are added. Typically P_{extup} is decreased from 6800 Pa to 5700 Pa (see Fig. 6). In that sense, the added non-linear losses imply the same kind of effect as an increase of the linear losses, that is an increase of β (Fig. 5). Again the playing range is influenced by the amount of losses.

[Figure 6 about here.]

As noted above, the main simplification of our approach is the direct translation of the quasi stationary models to the unsteady case. By using Eq. (20), the boundary condition at the open end of the pipe is symmetrical. That is, the non-linear loss term is the same for an out-going flow and an in-going flow. It is well known that the phenomena are asymmetrical (see for example Disselhorst [14]). The flow separation which occurs upon outflow is more pronounced than the one which occurs upon inflow. It is possible to take into account an asymmetrical effect by adapting the boundary condition, assuming for example that no non-linear losses occur upon inflow, Eq. (26), and twice the non-linear losses occur upon outflow, Eq. (27):

$$\text{if } v_s < 0 \quad \text{then} \quad p_s(t) = 0, \tag{26}$$

$$\text{if } v_s > 0 \quad \text{then} \quad p_s(t) = 2\left(\frac{c_d}{2}\right)\frac{1}{2}\rho v_s^2. \tag{27}$$

This situation should result in the same amount of losses as the previous one, Eq. (20). A simulation result using the asymmetrical boundary conditions is displayed in Fig. 6 for comparison with the one using the symmetrical boundary conditions. The envelopes corresponding to these two cases look similar. An interesting difference is that the mean pressure value is higher for the asymmetrical case than for the symmetrical case. However, it appears that the oscillation behaviour does not depend much on the way the quasi stationary model is translated to the unsteady case. In the following, all simulation results are based on Eq. (20) (symmetrical case).

3 Experiments

3.1 Experimental set-up and procedure

The artificial mouth consists of a Plexiglas box with metal reinforcement (Gazengel [24]). The artificial lip consists of a cylindrical latex balloon of small diameter (10 mm) in which a piece of foam saturated with water is inserted. The lip is fixed on a rigid support whose position can be translated vertically by means of a screw. This allows for variation of the reed opening at rest. The mouthpiece is inserted in a metal barrel

whose horizontal position can be adjusted. Resonators can be fixed onto the other end of the barrel. The air is supplied by a compressor through a pressure reducing valve.

The pressure P_m in the mouth is measured by a static pressure sensor (Druck PTX510). A miniature differential pressure sensor (Entran EPE-541-M) mounted in the wall of the mouthpiece measures the pressure difference $\Delta p = P_m - p$ between the mouth cavity and the inside of the mouthpiece.

The two pressure signals are stored in computer memory via a data acquisition card. The experiment starts without blowing pressure ($\Delta p = 0$). This state is maintained for a few seconds. This is done for the determination of the zeros of the pressure sensors. The pressure in the mouth cavity P_m is then increased gradually until the oscillation stops. Then, the reed completely closes the opening. This state is also maintained for a few seconds. This is done for the relative calibration of the differential pressure sensor measuring Δp: in that case $p = 0$ and then $\Delta p = P_m$. The sensitivity of the static pressure sensor measuring P_m is known, thus the sensitivity of the differential pressure sensor can be deduced. This calibration is necessary because the pressure in the mouthpiece p is obtained by making the difference between the signals from the two pressure sensors ($p = P_m - \Delta p$). Starting from a fully closed state, a second experiment is done, the pressure in the mouth being gradually brought back to zero. The typical duration of each experiment is 40 s with a sampling frequency of 2000 Hz. Instead of using a real clarinet, a tube 500 mm long and 16 mm wide is fitted to a clarinet mouthpiece and barrel. The termination of the tube can be adapted in order to vary the amount of non-linear losses. Two types of terminations are used. The first type of termination consists of pieces of tube with a circular flange of 25 mm diameter. They differ in their radius of curvature of the edges. Four radii of curvature r have been machined and used for the experiments, namely $r < 0.01$ mm, $r = 0.3$ mm, $r = 1$ mm, $r = 4$ mm. The second type of termination, which tends to approximate a pipe termination without thickness, has a sharp edge with a bevel angle of 20 ° (Fig. 7). These terminations have been extensively studied in [23] by measuring the real part of their impedance Z_{end} by means of a two microphone method. The measured terminations are the ones used in the experiments of the present paper. The results are displayed in Fig. 8. For each termination, the extra losses are roughly proportional to the acoustical velocity. The sharper the edges of the pipe termination are, the larger the losses become. Moreover, non-linear losses occur up to a certain velocity amplitude which increases as the edges become sharper.

[Figure 7 about here.]

[Figure 8 about here.]

In the present paper the amplitude of the acoustic pressure in the mouthpiece as a function of the mouth pressure is investigated. The amplitude as defined in the present paper is the amplitude of the signal, leaving

out the superimposed high frequency pressure fluctuations due to the mechanical resonance of the reed (see Fig. 9). In order to determine this amplitude, the root mean squared (RMS) value of the signal is calculated. The RMS value and the amplitude p are related by the following equation: $p = coeff.p_{RMS}$ where *coeff* is a coefficient depending on the shape of the signal. For a square signal $coeff = 1$ and for a sinusoidal signal $coeff = \sqrt{2}$. For the measured signals *coeff* is found to be $coeff = 1.10 \pm 0.05$. This value is valid for the beating reed regime, for different mouth pressures and for the different reed openings at rest investigated.

[Figure 9 about here.]

3.2 Estimation of the parameters for the simulations

In order to compare the experimental results with theoretical ones, the simulation method described in section 2 is used. The theoretical solutions resulting from the simulations depend on several parameters involved in the simplified model of the clarinet-like instrument. There are two kind of parameters, the ones linked with the reed-mouthpiece system, the others linked with the cylindrical resonator. This subsection is devoted to the determination of the values of these parameters.

The parameters linked with the reed-mouthpiece system are included in Eq. (5): the effective width of the reed channel w, the reed opening at rest H_0 and the reed stiffness k. The parameters k and w are directly estimated from previous measurements reported in Dalmont et al [25]: $k = 10700$ Pa/mm and $w = 12$ mm. The reed opening H_0 depends on the embouchure, that is the reed-mouthpiece adjustment of the artificial mouth. It is obtained from an experimental estimation of $P_M = kH_0$. P_M is assumed to be close to the threshold of oscillation P_{thdown} which is deduced from the experiment with decreasing pressure (see Figs. 12(a), 12(c) and 12(e)). Three embouchures have been analysed in this paper: a tight one ($P_M = 4000$ Pa), a medium one ($P_M = 5700$ Pa) and a slack one ($P_M = 8500$ Pa) which corresponds to $H_0 = 0.37$ mm, 0.53 mm, and 0.79 mm respectively.

The geometric parameters of the cylindrical resonator are directly estimated from the experimental set-up: the total length L equals 640 mm, the diameter D equals 16 mm. As assumed in section 2, two kind of losses are considered in this paper: the viscothermal losses in the pipe and the non-linear losses in its open end which are non-linear. Despite the frequency dependent nature of viscothermal losses, a dispersion-less model with a loss parameter independent of the frequency is used. The loss parameter is then assumed to be equal to the theoretical viscothermal loss parameter at the particular frequency 133 Hz which is a mean value of the fundamental frequencies obtained during the experiments using the artificial mouth. The viscothermal losses for a clarinet-like instrument sounding at 133 Hz, corresponding to a uniform pipe of length $L = 640$ mm and

diameter $D = 16$ mm, imply an amplitude transmission coefficient β on a travelling wave along the distance L equal to 0.97.

As detailed in section 2.2, the non-linear losses taken into account in the simulation involve a parameter c_d. The parameter c_d is deduced from the measurements of the real part of the terminal impedance Z_{end} (see Fig. 8): c_d is determined by estimating the mean slope of each of the curves displayed in Fig. 8, and by using Eq. (20). The results are reported in table 1. Indeed the model used in Eq. (20) is a great simplification of what occurs at the end of a pipe, and the determination of c_d is approximate. Moreover, Z_{end} has been derived from measurements with a harmonic excitation which leads to a quasi harmonic velocity at the end of the pipe. In a clarinet the excitation is not harmonic and the use of c_d in that case is somewhat questionable. However, as in a clarinet mouthpiece pressure signal the fundamental is dominating, the present approach is, at least qualitatively, sensible. This is a subject for further studies.

[Table 1 about here.]

3.3 Comparisons between the experimental results and the simulations

Experiments have been done in order to investigate the influence of the reed opening and the termination geometry on the playing range. It appears (see Figs. 10(a) and 10(b)) that the threshold of extinction P_{extup} is highly influenced by the reed opening, with a small reed opening leading to a small playing range. The threshold of extinction P_{extup} is around 4900 Pa, 9200 Pa, 12500 Pa for $H_0 = 0.37$ mm, 0.53 mm, and 0.79 mm respectively (see Fig. 10(a)). In each case the threshold of extinction P_{extup} is 25 to 60% larger than the threshold of oscillation P_{thdown} which is around 3900 Pa, 5800 Pa, 8200 Pa for $H_0 = 0.37$ mm, 0.53 mm, and 0.79 mm respectively (see Fig. 10(b)).

[Figure 10 about here.]

In order to do comparisons with the experiments, simulations are done using parameters obtained from experiments as described in section 3.2. In particular the value of P_M is obtained from experiments with decreasing pressure. It is verified that the threshold of oscillation with decreasing pressure is not influenced by the termination geometry. This justifies the assertion that P_{thdown} is approximately equal to P_M.

The comparisons are based on the investigation of the acoustic pressure amplitude in the mouthpiece as a function of the mouth pressure. The corresponding curves are displayed in two sets, a first set corresponding to an increasing mouth pressure (crescendo) is displayed Fig. 11, a second set corresponding to a decreasing mouth pressure (decrescendo) is displayed Fig. 12. In each set, the experimental results are displayed on the

left hand side of the figure, the simulation results on the right hand side. On each side, the three embouchures defined in section 3.2 are displayed separately (from top to bottom, tight embouchure, medium embouchure and slack embouchure). In each of the 6 graphs per figure, curves corresponding to the different terminations are displayed. All experiments and simulations are based on the analysis of the first oscillation regime of the clarinet-like system (playing frequency around 133 Hz). From the experimental point of view, it is not easy to get the same oscillation regime for every embouchure and every mouth pressure value. Actually, the experimentally observed behaviour is sometimes the second oscillation regime instead of the first one, particularly during the crescendo case: the oscillation first reaches the second regime and then is forced to reach the first regime a twelfth below, from the mouth pressure middle range until the saturation. As a consequence Figs. 11(c) and 11(e) show troubled curves around $P_m = 4500$ Pa and $P_m = 6000$ Pa respectively. It is inconsequential here as the present study is focused on the saturation mechanism. Notice that the first oscillation regime is obtained without difficulty for each of the decrescendo cases (Figs. 12(a), 12(c) and 12(e)).

[Figure 11 about here.]

Experiments show that the extinction threshold is significantly influenced by the termination geometry. The termination with the more rounded edges leads to the larger playing range. In contrast, the termination with sharp edges leads to the smaller playing range. This is easily explained by the fact that sharp edges lead to a high non linear loss coefficient. This is confirmed for the three embouchures by simulations. From the musical point of view, the dynamic level and the playing range are increased when the losses are minimised. The maximum amplitude of the oscillation depends on the amount of losses: typically a significant difference of 10% of the mouth pressure on the oscillation amplitude is experimentally observed between the unflanged termination and the most rounded termination (curvature $r = 4$ mm) for all three embouchures. This is theoretically observed too, but the simulation results show a larger amplitude difference: a difference about 30% is shown on the Figs. 11(b), 11(d) and 11(f). On the contrary, the amplitude of the oscillations in the decreasing pressure does not depend much on the amount of losses. This can simply be explained by the fact that in this situation ($P_m < P_M$) non linear losses effects remain small because the acoustic velocity at the end of the pipe is still small.

[Figure 12 about here.]

4 Conclusion and prospects

Our work shows that the lossless model as described in section 2 used for studying oscillations of the clarinet [4, 7, 29] needs to be extended. Indeed, with this model, there is no limit to the amplitude of the oscillations, so it is not able to determine the playing range of an instrument. Losses need to be included in the model. It is shown by doing time domain simulations that frequency independent linear losses are sufficient to describe qualitatively the saturation phenomenon observed experimentally using an artificial mouth. The extinction mouth pressure is decreasing when the amount of losses is increasing during a crescendo process. In contrast, during a decrescendo process the threshold of oscillation is not significantly influenced by losses. This shows an inverse bifurcation scheme where the losses play a decisive role. Analytical developments could be done to determine the bifurcation diagram of a simplified clarinet at the saturation. Such a study could also be extended to conical instruments such as the saxophone. In that case analytical developments using stepped cone models are probably also possible in order to determine the bifurcation diagrams. As suggested in [12] this would make it possible to explain how the inverted Helmholtz motion, which is shown in [34] to be stable in the beating reed regime, can appear.

On the other hand the present simulations and experiments show that non linear losses have a significant influence on the playing range of a clarinet. Especially it is shown that rounded edges may increase the playing range. This may be related to some instrument makers practice which consist to drill conical holes instead of cylindrical holes. However, the question of a tube with side holes is different from the problem studied here because side holes usually have a diameter significantly smaller than the diameter of the pipe, which would lead to larger non linear losses (see [20]). Moreover, the fact that more than one hole is open make the problem more complex [22].

The influence of the non-linear losses on the acoustical pressure amplitude has been shown; their influence on the spectrum and pressure waveform of a clarinet could also be investigated. Indeed comparison between experiments and theory including viscothermal losses show significant discrepancies [35]. Non linear losses may explain some of the differences.

Acknowledgements

The authors would like to thank S. Collin for the machining of the terminations, E. Ducasse and M. van Walstijn for fruitful discussions.

References

[1] C.J. Nederveen. *Acoustical aspects of woodwind instruments.* Northern Illinois University Press, 1998.

[2] N.H. Fletcher and T.D. Rossing. *The physics of musical instruments.* Springer–Verlag, 1998.

[3] A. Hirschberg. Aero-acoustics of wind instruments. In *Mechanics of Musical Instruments*, volume 355 of *CISM courses and lectures.* Springer–Verlag, Wien, 1995.

[4] J. Kergomard. Elementary considerations on reed-instruments oscillations. In *Mechanics of Musical Instruments*, volume 355 of *CISM courses and lectures.* Springer–Verlag, Wien, 1995.

[5] W.E. Worman. *Self-sustained non-linear oscillations of medium amplitude in clarinet-like systems.* PhD thesis, Case Western University, Cleveland, Ohio, 1971.

[6] A.H. Benade and S.N. Kouzoupis. The clarinet spectrum : theory and experiment. *J. Acoust. Soc. Am.*, 83(1):292–304, 1988.

[7] M.E. Mc Intyre, R.T. Scumacher, and J. Woodhouse. On the oscillations of musical instruments. *J. Acoust. Soc. Am.*, 74:1325–1345, 1983.

[8] N. Grand, J. Gilbert, and F. Laloë. Oscillation threshold of woodwinds instruments. *Acta Acustica*, 1:137–151, 1997.

[9] J.-P. Dalmont, J. Gilbert, and J. Kergomard. Reed instruments, from small to large amplitude periodic oscillations and the Helmholtz motion analogy. ACUSTICA - *Acta Acustica*, 86(4):671–684, 2000.

[10] A.H. Benade. *Fundamentals of Musical Acoustics.* Dover (New York), 1976.

[11] A.H. Benade and J.K. Cuddeback. Quasi-turbulent damping at wind instrument joints and tone holes. *J. Acoust. Soc. Am.*, 55(1):457–, 1973.

[12] J.-P. Dalmont, E. Ducasse, and S. Ollivier. Saturation mechanism in reed instruments. In *3rd EEA European Congress on Acoustic.* Sevilla, 2002.

[13] U. Ingard and S. Labate. Acoustic circulation effects and the nonlinear impedance of orifices. *J. Acoust. Soc. Am.*, 22(2):211–218, 1950.

[14] J.H.M. Disselhorst and L. Van Wijngaarden. Flow in the exit of open pipes during acoustic resonance. *J. Fluid Mech.*, 99(2):293–319, 1980.

[15] M.C.A.M. Peters, A. Hirschberg, A.J. Reijnen, and A.P.J. Wijnands. Damping and reflection coefficient measurements for an open pipe at low Mach and low Helmholtz numbers. *J. Fluid Mech.*, 256:499–534, 1993.

[16] H. Bouasse. *Instruments à vent.* Delagrave, 1929.

[17] J.W. Coltman. Sounding mechanism of the flute and organ pipe. *J. Acoust. Soc. Am.*, 44:983–992, 1968.

[18] D.H. Keefe. Physical modelling of wood instruments. *Computer Music Journal*, 16(4):57–73, 1992.

[19] A.H. Benade and D.H. Keefe. The physics of a new clarinet design. *Galpin Society Journal*, pages 113–142, 1996.

[20] J.-P. Dalmont, C.J. Nederveen, V. Dubos, S. Ollivier, V. Méserette, and E. te Sligte. Experimental determination of the equivalent circuit of a side hole: linear and non-linear behaviour. ACUSTICA - *Acta Acustica*, 88(4):567–575, 2002.

[21] M. Castellengo and L. Forest. Métamorphoses de la flûte traversière au 19éme siècle : esthétique musicale, acoustique et facture. In Cité de la musique, editor, *Acoustique et instruments anciens*, pages 85–100, Paris, 1998. SFA.

[22] J.-P. Dalmont, E. Ducasse, and S. Ollivier. Practical consequences of tone holes non-linear behaviour. In *Proceedings of the International Symposium on Musical Acoustics*, pages 153–156. Perrugia, 2001.

[23] M. Atig, J.-P. Dalmont, and J. Gilbert. Termination impedance of open-ended cylindrical tubes at high sound pressure level. *C. R. Mécanique*, 2003. Submitted.

[24] B. Gazengel. *Caractérisation objective de la qualité de justesse, de timbre et d"émission des instruments à vent à anche simple.* PhD thesis, Université du Maine, Le Mans, France, 1994.

[25] J.-P. Dalmont, J. Gilbert, and S. Ollivier. Non-linear characteristics of single reed instruments : quasi-static volume flow and reed opening measurements. *J. Acoust. Soc. Am.*, 2003. Accepted for publication.

[26] J.-P. Dalmont, B. Gazengel, J. Gilbert, and J. Kergomard. Some aspects of tuning and clean intonation in reed instruments. *Applied Acoustics*, 46:19–60, 1995.

[27] S. Ollivier, J.-P. Dalmont, and J. Kergomard. Idealized models of reed woodwinds. part I : analogy with the bowed string. *Acustica*, 2002. Submitted.

[28] R.T. Schumacher. Ab initio calculations of the oscillation of a clarinet. *Acustica*, 48:71–85, 1981.

[29] C. Maganza. *Excitations non-linéaires d'un conduit acoustique cylindrique. Observations de doublements de période précédent un comportement chaotique. Application à la clarinette.* PhD thesis, Université du Maine, Le Mans, France, 1985.

[30] P. Berge, Y. Pomeau, and C. Vidal. *Order within Chaos : Towards a Deterministic Approach to Turbulence.* John Wiley & Sons, 1987.

[31] J. Guckenheimer and P. Holmes. *Nonlinear Oscillations, Dynamical Systems, and Bifurcations of Vector Fields*, volume 42 of *Applied Mathematical Sciences.* Springer Verlag, 1997.

[32] U. Ingard and H. Ising. Acoustic nonlinearity of an orifice. *J. Acoust. Soc. Am.*, 42(1):6–17, 1967.

[33] S. Ollivier and J.-P. Dalmont. Mise en évidence d'une non-linéarité localisée au niveau d'un trou latéral d'instrument à vent. In *Vème Congrès Français d'Acoustique*, pages 310–313, Lausanne, Septembre 2000.

[34] S. Ollivier, J. Kergomard, and J.-P. Dalmont. Idealized models of reed woodwinds. part II : on the stability of two-step oscillations. *Acustica*, 2002. Submitted.

[35] S. Ollivier. *Contribution à l'étude des oscillations des instruments à vent à anche simple.* PhD thesis, Université du Maine, Le Mans, France, 2002.

List of Figures

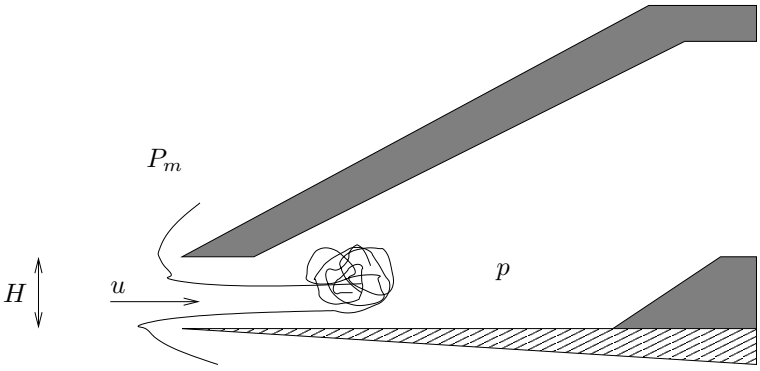

Figure 1:

Figure 2: Positive and negative going plane wave pressures at the input (p_e^+ and p_e^- respectively) and at the open end of the pipe (p_s^+ and p_s^- respectively)

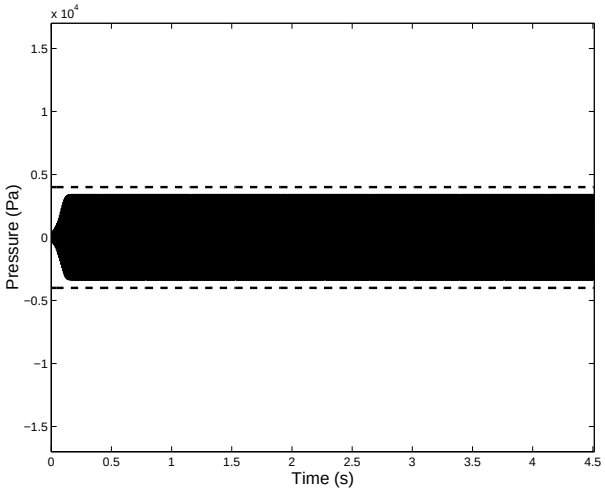

(a) Constant mouth pressure equal to 4000 Pa

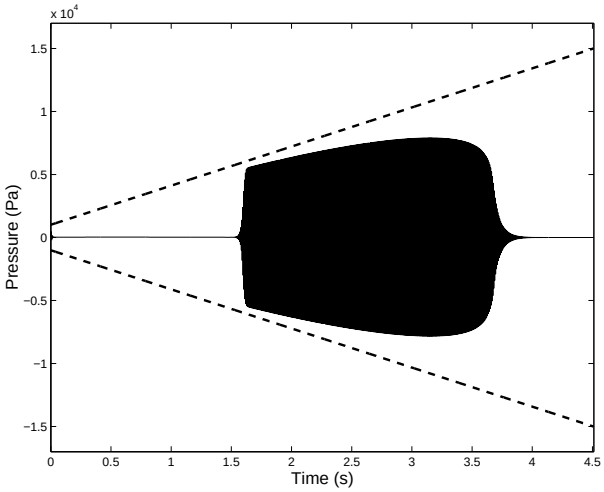

(b) Crescendo using a mouth pressure varying from 150 Pa to 15000 Pa in 4.5 s

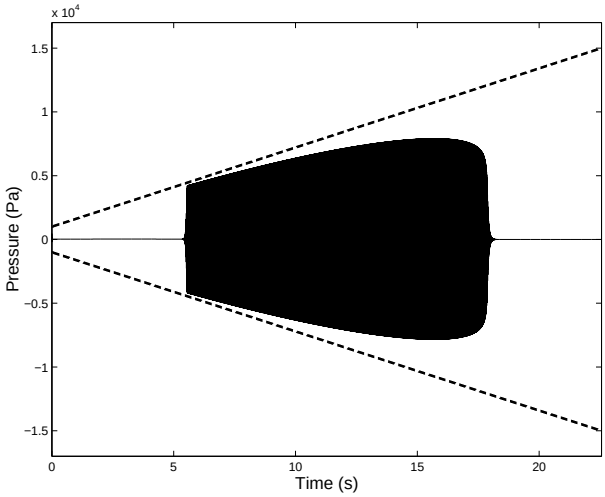

(c) Crescendo using a mouth pressure varying from 150 Pa to 15000 Pa in 22.5 s

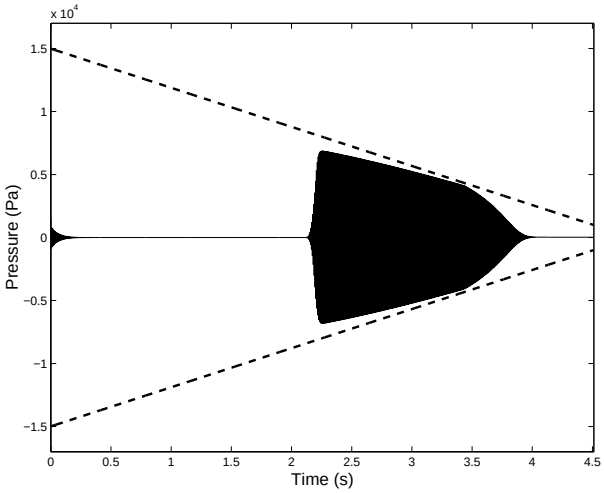

(d) Decrescendo using a mouth pressure varying from 15000 Pa to 150 Pa in 4.5 s

Figure 3:

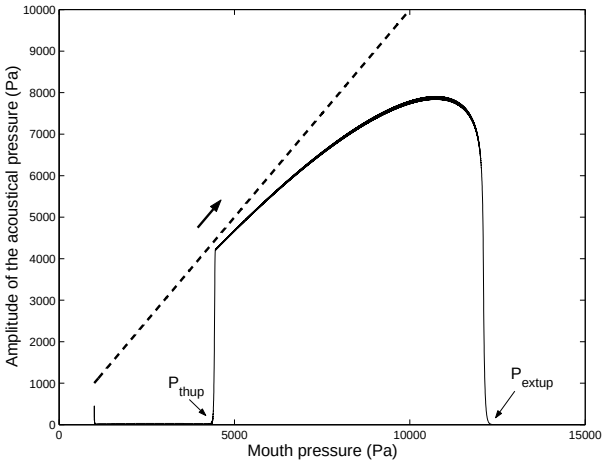

(a) Amplitude of the simulated acoustical pressure as a function of the mouth pressure

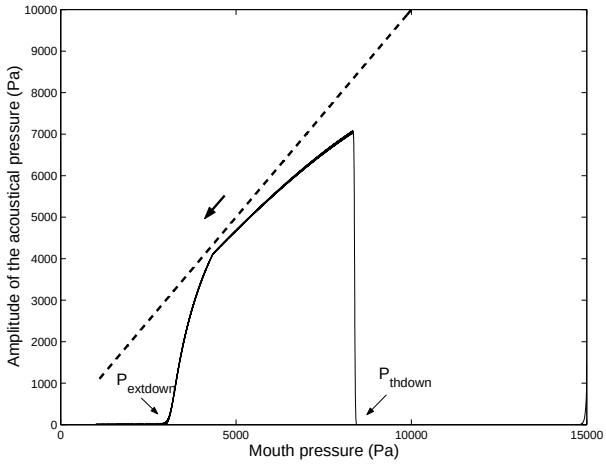

(b) Amplitude of the simulated acoustical pressure as a function of the mouth pressure

Figure 4:

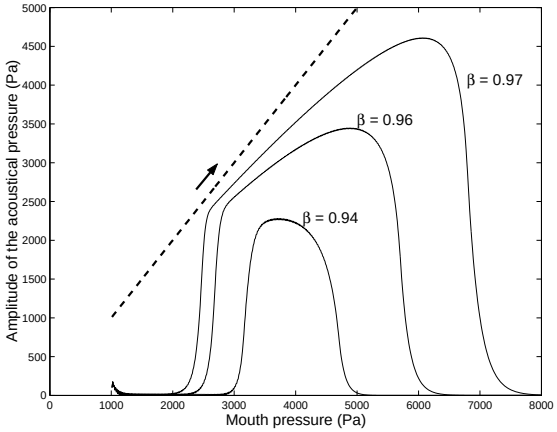

(a) Crescendo from 150 Pa to 15000 Pa.

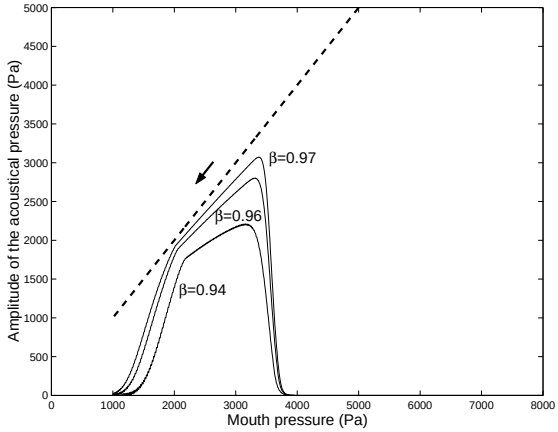

(b) Decrescendo from 15000 Pa to 150 Pa.

Figure 5:

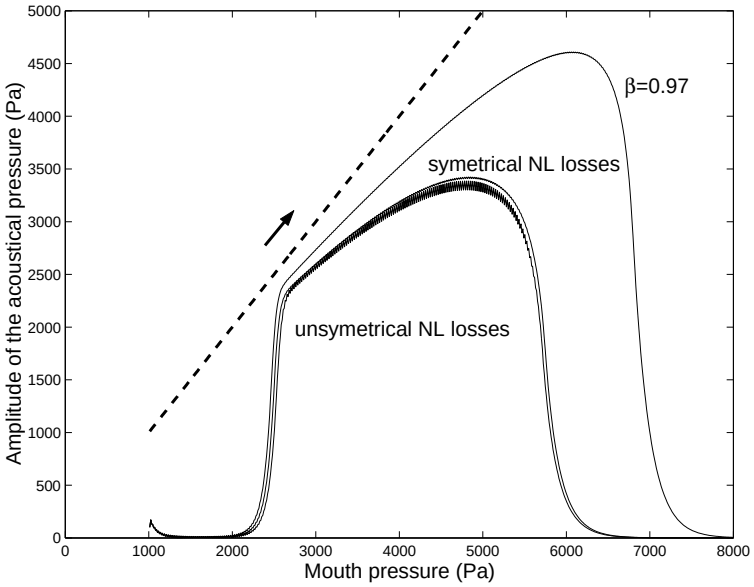
Amplitude of the acoustical pressure (Pa)
Mouth pressure (Pa)
β=0.97
symetrical NL losses
unsymetrical NL losses
0
500
1000
1500
2000
2500
3000
3500
4000
4500
5000
0
1000
2000
3000
4000
5000
6000
7000
8000

Figure 6:

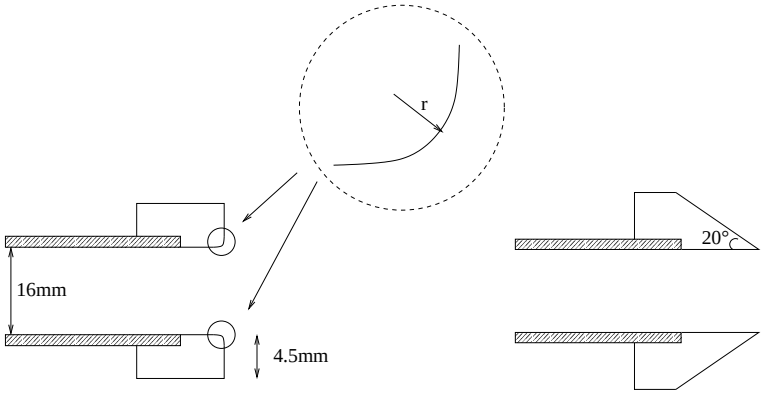

Figure 7:

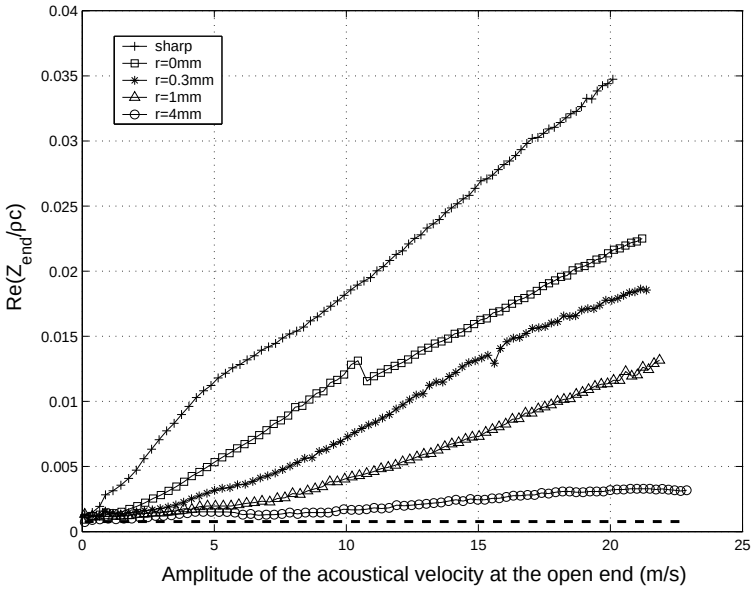
sharp
r=0mm
r=0.3mm
r=1mm
r=4mm
Re(Z_end/ρc)
Amplitude of the acoustical velocity at the open end (m/s)
0.04
0.035
0.03
0.025
0.02
0.015
0.01
0.005
0
0
5
10
15
20
25

Figure 8:

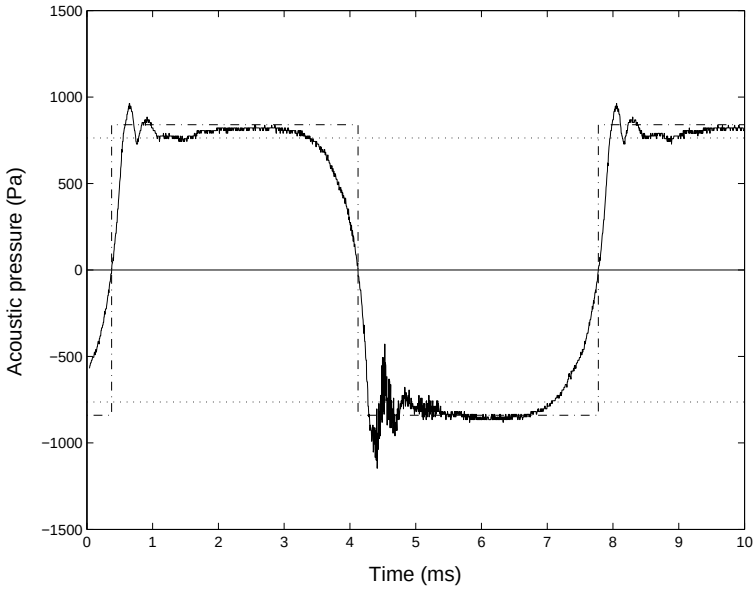
1500
1000
500
0
−500
−1000
−1500
Acoustic pressure (Pa)
0
1
2
3
4
5
6
7
8
9
10
Time (ms)

Figure 9:

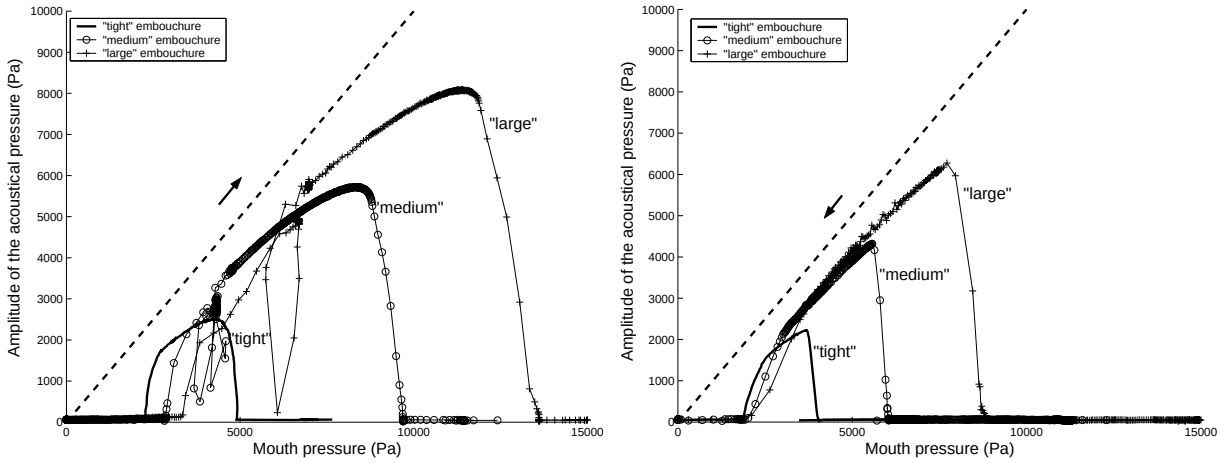

(a) Crescendo.

(b) Decrescendo.

Figure 10:

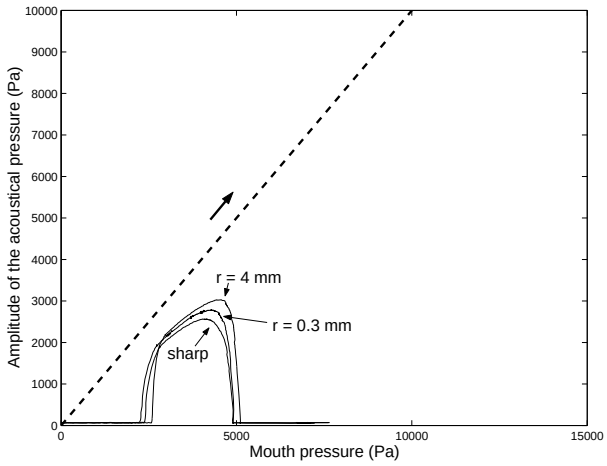

(a) Experiment, crescendo, tight embouchure.

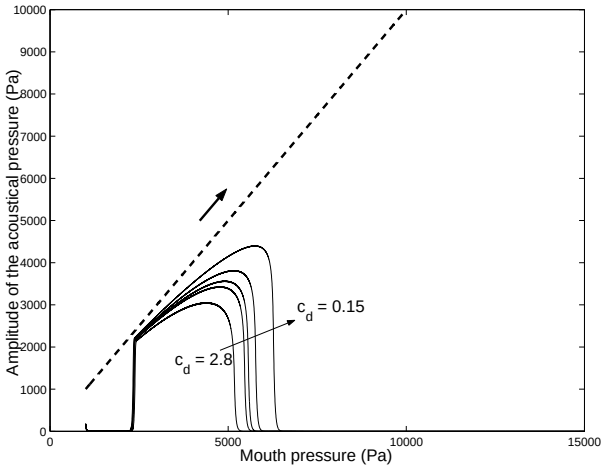

(b) Simulation, crescendo, tight embouchure (P_M = 4000 Pa).

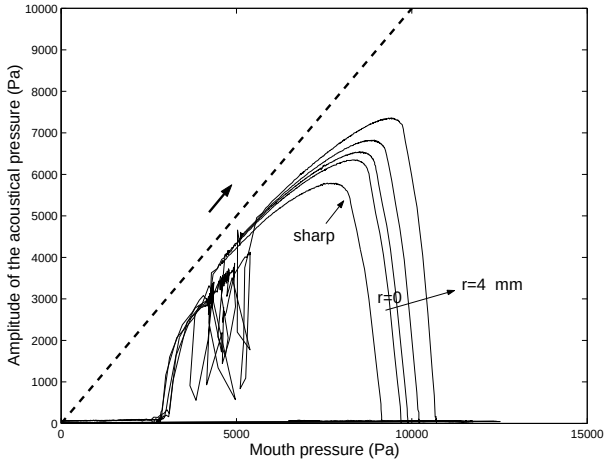

(c) Experiment, crescendo, medium embouchure.

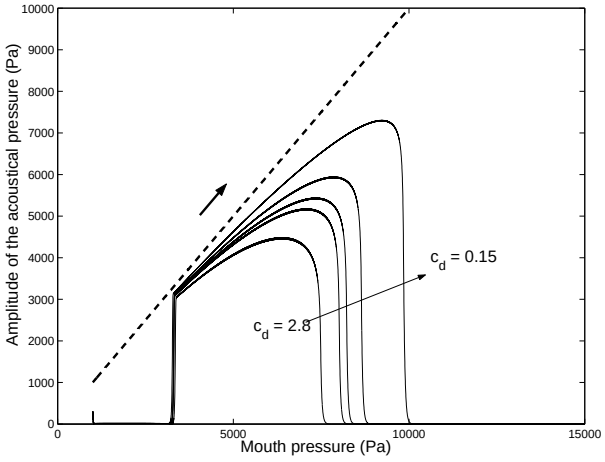

(d) Simulation, crescendo, medium embouchure (P_M = 5700 Pa).

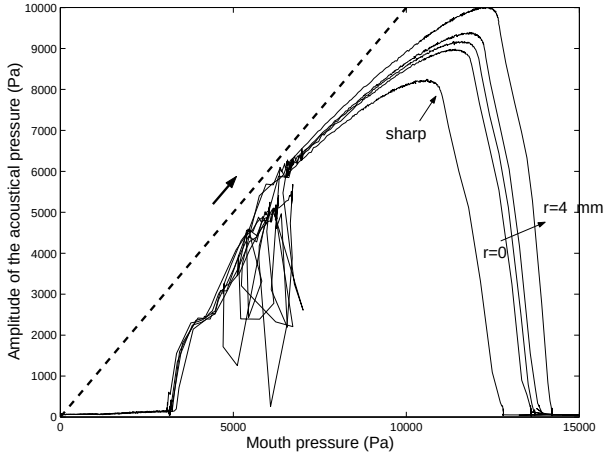

(e) Experiment, crescendo, large embouchure.

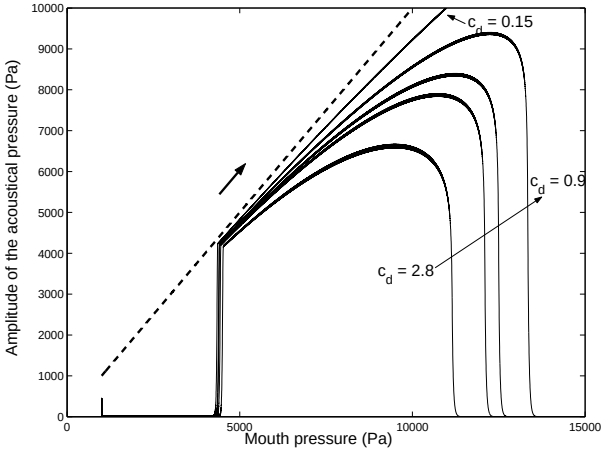

(f) Simulation, crescendo, large embouchure (P_M = 8500 Pa).

Figure 11:

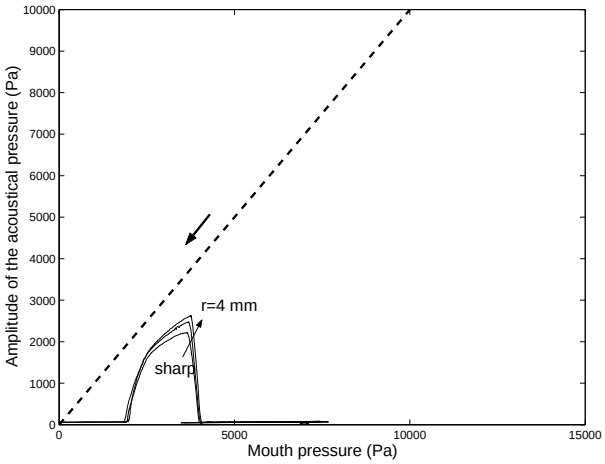

(a) Experiment, decrescendo, tight embouchure.

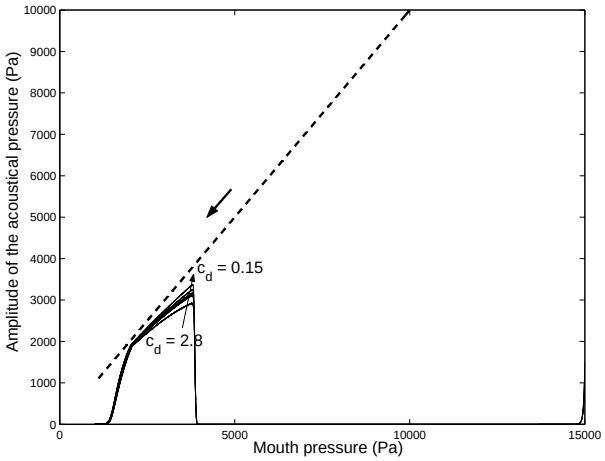

(b) Simulation, decrescendo, tight embouchure ($P_M = 4000$ Pa).

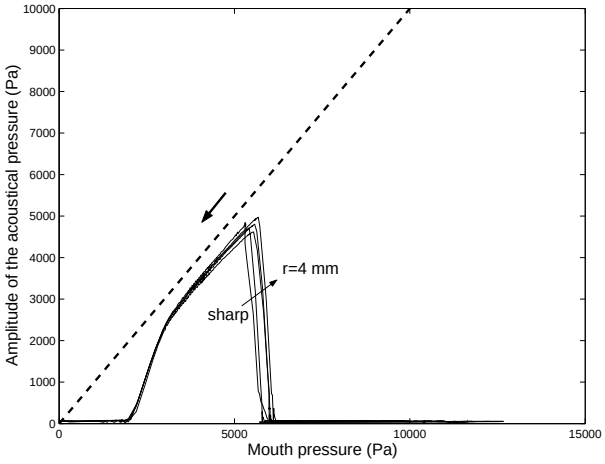

(c) Experiment, decrescendo, medium embouchure.

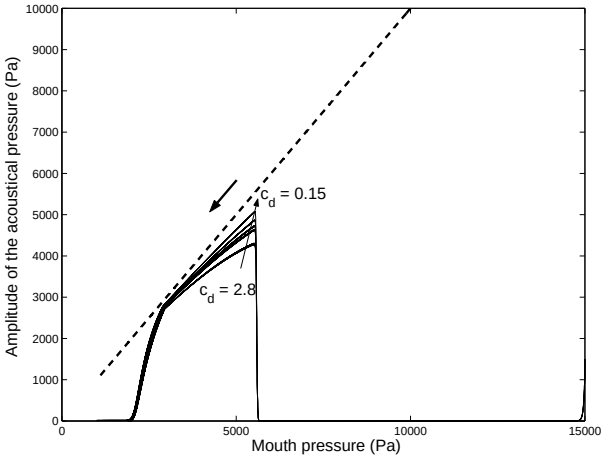

(d) Simulation, decrescendo, medium embouchure ($P_M = 5700$ Pa).

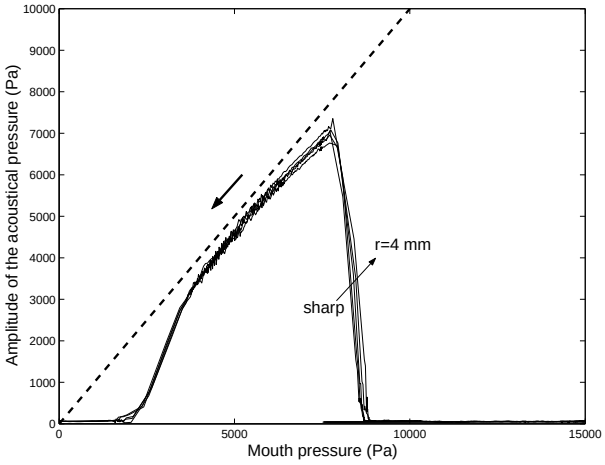

(e) Experiment, decrescendo, large embouchure.

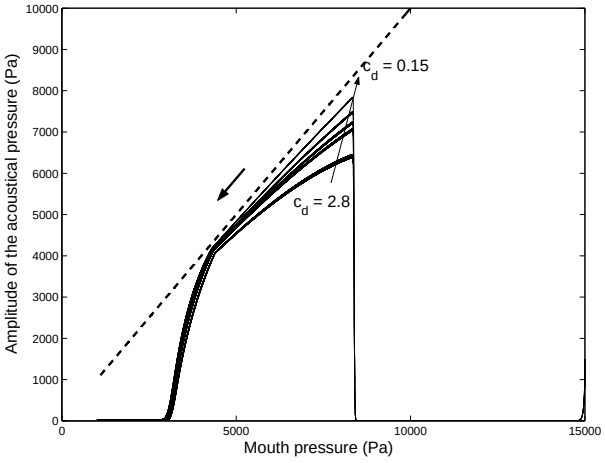

(f) Simulation, decrescendo, large embouchure ($P_M = 8500$ Pa).

Figure 12:

List of Tables

Table 1: Experimental values of the parameter c_d

Termination geometry (see Fig. 7)	Parameter c_d
Unflanged pipe termination with sharp edges	2.8
Flanged termination with a radius of curvature $r < 0.01$ mm	1.7
Flanged termination with a radius of curvature $r = 0.3$ mm	1.4
Flanged termination with a radius of curvature $r = 1$ mm	0.9
Flanged termination with a radius of curvature $r = 4$ mm	0.15